PROCEEDINGS OF SCIENCE

Localisation and chiral symmetry in 2+1 flavour domain wall QCD

RBC and UKQCD Collaborations

D. J. Antonio, K. C. Bowler, P. A. Boyle*, M. A. Clark, B. Joo, A. D. Kennedy, R. D. Kenway, C. M. Maynard, R. J. Tweedie

School of Physics,
Edinburgh University
Edinburgh, EH9 3JZ, UK
E-mail: dja@ph.ed.ac.uk, kcb@ph.ed.ac.uk, paboyle@ph.ed.ac.uk, mike@ph.ed.ac.uk, bj@ph.ed.ac.uk, adk@ph.ed.ac.uk, r.d.kenway@ed.ac.uk, cmaynard@ph.ed.ac.uk, rjt@ph.ed.ac.uk

A. Yamaguchi

Department of Physics and Astronomy,
Glasgow University
University Avenue,
Glasgow G12 8QQ, UK
E-mail: azusa@physics.gla.ac.uk

We present results from QCDOC for the dependence of the residual mass on the size of the fifth dimension, and its relation to the density and localisation properties of low eigenvectors of the Hermitian Wilson Dirac operator and the domain wall transfer matrix, for 2+1 flavour domain wall QCD using DBW2 and Iwasaki gauge actions. Using ensembles of $16^3 \times 32$ configurations, with an extent of 8 in the fifth dimension for the sea quarks, we demonstrate the existence of a regime where locality, chiral symmetry breaking and topology change can be acceptable for inverse lattice spacings $a^{-1} \geq 1.6$ GeV.

XXIIIrd International Symposium on Lattice Field Theory
25-30 July 2005
Trinity College, Dublin, Ireland

*Speaker.

PoS(LAT2005)141

1. Introduction

All current formulations of lattice chiral symmetry in one way or another use a negative mass Wilson-like Hermitian Dirac operator, $H_W = \gamma_5 D_W$, of the Kaplan approach [1]. Various procedures are used to modify the spectrum to display either exact (to machine and convergence precision), or in the case of DWF exponentially accurate, chiral symmetry. The structure of the Aoki phase of this negative mass Wilson operator has direct implications for the appropriate regions of parameter space in which to simulate light dynamical fermions. A modification [2] of the argument of Hernandez et al [3] shows that a gap in the spectrum of *extended* states of H_W guarantees locality of the resulting chiral operator. Numerical evidence suggests that, at affordable couplings, there is a gap in the spectrum of extended states, but the spectrum is filled with a non-zero density of localised states. It is prudent only to accept a density of low modes in the simulation ensemble when accompanied by a demonstration of this eigenmode structure. Further, in domain wall and related approaches, the residual chiral symmetry breaking effects depends in detail on the densities and sizes of modes of the transfer matrix. In fact a model of this dependence will be used as one of several diagnostics to investigate the nature of the spectrum in our simulations.

This strong coupling behaviour of Wilson fermions does not leave one at liberty to simulate QCD at arbitrarily coarse lattice spacings. Simple categorisation of errors in a weak coupling expansion in a and α_s will break down near the phase boundary, which bounds the coarsest lattice spacing at which the formulation makes sense. This implies a minimum cost that must be paid for a given class of action to have the formulation under control. The phase boundary is action dependent, and, while the negative mass Wilson kernel does not normally weight the ensemble its zero modes are the same as those of the transfer matrix. So for the first time we perform a numerical study of the localisation of its low modes in the real-world case of 2+1 flavours of *dynamical* (almost) chiral fermions and demonstrate that 2+1 flavour dynamical DWF simulations are rendered affordable to the RBC and UKQCD collaborations by our new QCDOC systems.

2. Aoki phase diagram of lattice QCD

The history of the Aoki phase is both rich and interesting. The phase was first conjectured and described by Aoki [4] in both the quenched and dynamical cases. The order parameter for the phase is a pionic condensate. This condensate spontaneously breaks flavour-parity in the two flavour dynamical case, with a flavour non-singlet Goldstone pion for dynamical Wilson fermions throughout the Aoki phase. In the single-flavour quenched case, (discrete) parity is spontaneously broken, and the massless mode that arises is a pseudo-pion on the critical line of the Aoki phase transition, but may be massive in portions of the phase. Since the Hermitian Wilson Dirac operator has a Banks-Casher relation a non-zero density of near-zero modes is associated with the condensate in both the quenched and dynamical cases.

It was observed [5, 6] that the quenched Aoki phase consists of two qualitatively different regions bounded by a critical $\beta_c(M_5)$. Below $\beta_c(M_5)$ near-zero modes are delocalised and, above $\beta_c(M_5)$, the phase contains localised near-zero modes. In both regions the pionic condensate and density of near-zero modes are non-zero, but their localisation properties differ fundamentally.

Golterman et al [2] introduced to QCD the concept of a non-zero mobility edge λ_c, as a critical eigenvalue of H_W Dirac operator above which all eigenstates are extended and below which states

are localised. They also applied the Mckane and Stone localisation escape from Goldstone's theorem to lattice QCD at non-zero lattice spacing in the two-flavour quenched case. Specifically, they showed that two quenched flavours with a non-zero mobility edge can display a spontaneous breaking of a continuous local symmetry *without* a corresponding Goldstone boson. This observation is key to the correct functioning of all the various formulations of Kaplan fermions wherever the kernel H_W has a non-zero density of low modes. This qualitative picture is displayed in Figure 1.

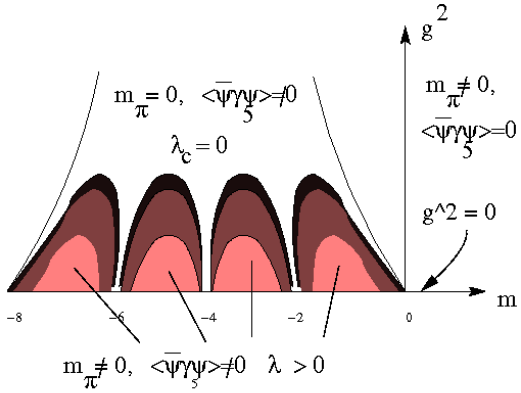

Figure 1: Schematic diagram of the quenched Aoki phase. A pionic condensate and corresponding non-zero density of near zero modes is developed throughout most of the negative mass region. In the coloured sectors, a non-zero mobility edge is developed and the contours could equally well represent either decreasing low mode density, decreasing pionic condensate or increasing λ_c as one moves towards the continuum limit at $g^2 = 0$.

3. Implications for residual chiral symmetry breaking in DWF

For domain wall and related approaches the form of the spectrum of the transfer matrix has implications the approximation to chiral symmetry, which we analyse via the axial Ward identity defect,

$$m_{\rm res} = \frac{\sum_y \langle J_5(y,t) P(0)\rangle}{\sum_y \langle P(y,t) P(0)\rangle} \tag{3.1}$$

where J_5 is the usual point-split midpoint pseudoscalar density, and P is the pseudoscalar density on the walls.

The log of the transfer matrix in the 5th dimension is H_T, and this operator will have a mobility edge λ_T. In correlation functions, a volume factor suppresses localised states, giving two forms [2, 7] of leading contribution to $m_{\rm res}$, each with an infrared shell cutoff of $O(\frac{1}{L_s})$:

$$m_{\rm res}(L_s) = \left(c_1 e^{-\lambda_T L_s} + c_2\right) \frac{1}{L_s} \tag{3.2}$$

these contributions are respectively: (i) exponentially suppressed in L_s; volume enhanced states at mobility edge $\lambda_T \leq \lambda \leq \lambda_T + \frac{1}{L_s}$, and (ii) poorly suppressed in L_s; low lying localised states with $\lambda \leq \frac{1}{L_s}$. Here c_2 is proportional to the density of near-zero modes, $\rho(0)$, and we require a demonstrably non-zero mobility edge λ_T for safe QCD simulations with chiral formulations. It is acceptable to have a significant non-exponential component in $m_{\rm res}$. Formally one should extrapolate to $L_s = \infty$ to remove residual chiral symmetry breaking effects, but practically it is only necessary that $m_{\rm res}$ be numerically small compared to the smallest explicit quark mass in the simulation, and chiral symmetry breaking effects absorbed with an additive mass renormalisation. Taking $\frac{1}{10}$ our lightest mass at current lattice spacings suggests $m_{\rm res} = O(10^{-3})$ as adequate.

We show fits to the functional form 3.2 for three degenerate flavour ensembles at several gauge couplings for the Iwasaki and DBW2 gauge actions in figure 2, and the fitted parameters in table 1.

Figure 2: Valence $m_{\rm res}(L_s)$ dependence of partially quenched DWF with the DBW2 and Iwasaki gauge actions as a function L_s using $L_s = 8$ and the indicated β values on a $16^3 \times 32$ volume for the ensembles. The sea and valence quark masses are 0.04 throughout.

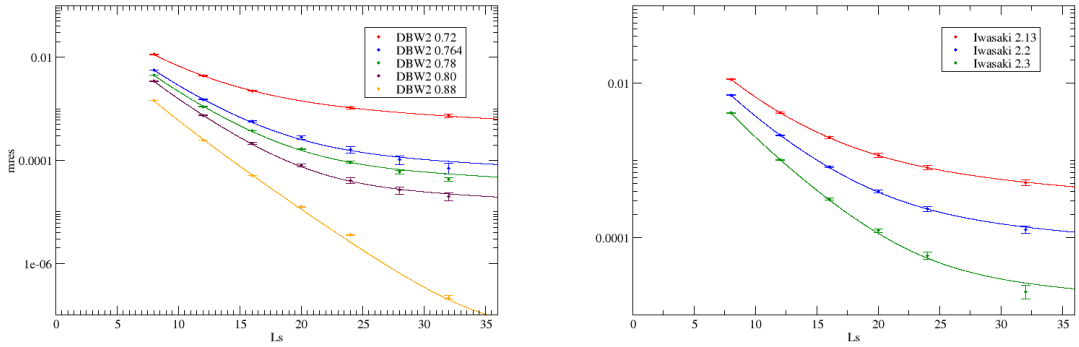

Table 1: Fit parameters to the dependence of $m_{\rm res}$ on L_s shown in figure 2. We also give the lattice spacing obtained from a the static potential [9] dynamical background $m_{ud} = m_s = 0.04$ without chiral extrapolation. This differs from lattice spacing defined in the chiral limit presented elsewhere in this conference, and we only provide the lattice spacings here for illustration.

Iwasaki β	c_1	λ_c	$c_2 \simeq \rho(0)$	a^{-1}
2.13	0.35	0.195(1)	0.0160(1)	1.61(2)
2.2	0.30	0.221(1)	0.0041(3)	1.89(3)
2.3	0.24	0.254(1)	0.0007(1)	-

DBW2 β	c_1	λ_c	$c_2 \simeq \rho(0)$	a^{-1}
0.72	0.35	0.204(1)	0.0225(3)	1.40(4)
0.764	0.31	0.25(1)	0.0029(1)	1.74(2)
0.78	0.28	0.26(1)	0.0017(2)	1.81(4)
0.80	0.27	0.291(3)	0.00069(5)	1.98(4)
0.88	0.16	0.33(1)	$\leq 2e^{-6}$	-

4. Microscopic study of the mobility edge

We will now compare the above ensemble averaged determination of the mobility edge to a microscopic view based on the size distribution of individual eigenvectors. We determined up to 256 eigenvectors of H_W using the CHROMA code base , on 25 configurations per ensemble. For each eigenvector, $\psi(x)$, we define a localisation length in a robust way as follows. Defining (i) mode density $\rho(x) = \psi^\dagger\psi(x)$ and center x_0 such that $\rho(x_0) \geq \rho(x) \forall x \neq x_0$; (ii) radius $r(x) = |x - x_0|$ using nearest periodic mirror image; (iii) effective localisation exponent $L_{\rm eff}(x) = \frac{2r(x)}{\log\rho(x_0) - \log\rho(x)}$; and (iv) robust localisation length $L_{\rm max} = \max_{r(x)\geq 5} L_{\rm eff}(x)$.

As the eigenvalue approaches the mobility edge from below, we observed two clear processes by which delocalisation takes place. Firstly, the mean rate of fall off from the center decreases creating much bigger states. Secondly, states become increasingly multi-centered, with exponential fall off between a number of satellite peaks. The above definition of localisation length is designed to reflect both the process of single peak broadening, and the development of multiple peaks. Inverse participation ratios, for example, would be a less robust measure of locality in that it would not differentiate two well separated δ functions from those on two neighbouring sites. We display scatter plots of this definition of localisation length in Figure 3 for the Iwasaki and DBW2 gauge actions at $\beta = 2.13$ and $\beta = 0.764$ respectively.

We computed the lowest 10 modes of the 5d Hermitian domain wall operator $H_{\rm DWF} = \gamma_5 R_5 D_{\rm DWF}$

Figure 3: Microscopic view of the mobility edge based on a scatter plot of maximal localisation lengths of individual low eigenmodes of H_W. We overlay the mobility edge determinations for the H_T mobility edge from fits to the model for $m_{\rm res}$ and find good agreement for both the Iwasaki and DBW2 gauge actions.

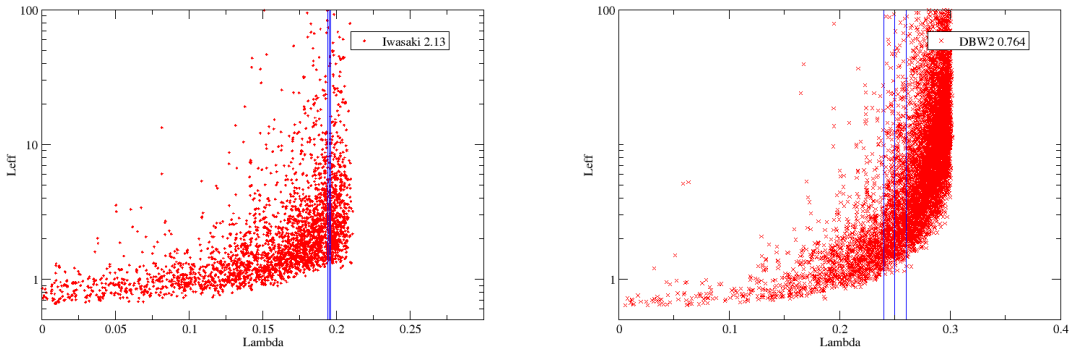

Figure 4: We display an iso-surface through the eigenvector density of a chiral mode bound to the wall. Here s is the vertical direction, t the left-right axis, and z runs into the page. Two different values of x and y are shown $(3,3)$ and $(11,13)$ showing both a localised incursion of the eigenmode associated with a low mode of H_W, and a uniformly well stuck region.

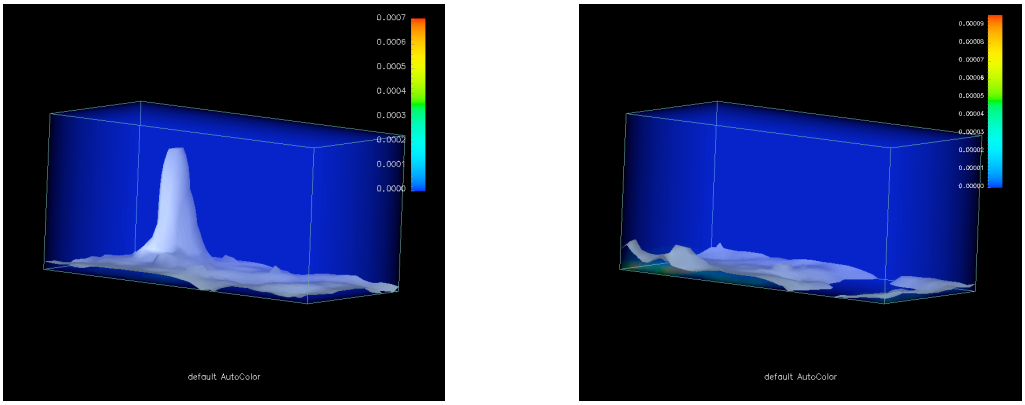

using the Columbia Physics System on a single configuration from a $16^3 \times 32 \times 8$ DBW2 2+1 flavour ensemble at $\beta = 0.764$. The role of localised low modes of H_W providing conduits into the bulk for chiral symmetry breaking and causing corresponding localised spikes in the correlation function for $m_{\rm res}$ is corroborated by the iso-surfaces of constant eigenvector density obtained in our simulation in figure 4. A movie, raster scanning x and y as a unified "movie-time", can be obtained from http://www.ph.ed.ac.uk/~paboyle/QCD/5dmode.mpg On the same configuration, we used the lowest 256 eigenmodes of the 4d Hermitian Wilson operator computed using the CHROMA system to expres the 5d modes as a sum over 4d modes using $\Psi_i(x,s) = N_s \sum_j \alpha_{ij} \psi_j(x)$, where $N_s^2 = \sum_x \Psi_i^\dagger(x,s)\Psi_i(x,s)$ normalises each s-slice. If the basis were complete $\sum_j \alpha_{ij}^2 = 1$, however this can only be true in the bulk for large L_s, so we computed 5d modes for a valence $L_s = 16$, and not the unitary $L_s = 8$ point, finding that for that while the basis is incomplete on the wall the description of the propagation in the bulk is as much as 80% complete despite the mismatch between H_T and H_W. A few low 4d modes almost completely describe the coupling between walls for each 5d mode. The coefficients α_{ij} for a typical chiral mode are displayed in figure 5 and it can be seen

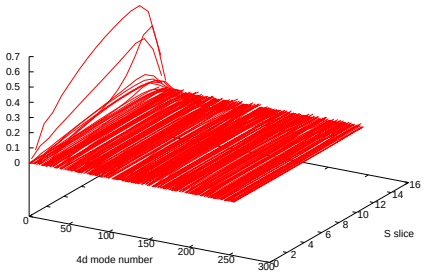

Figure 5: Normalised overlap of different s-slices of a chiral 5d eigenmode of H_{DWF} with the first 256 4d eigenmodes of H_W. We take the valence operator with $L_s = 16$, and demonstrate numerically that only a few low-lying 4d eigenmodes dominate the large L_s contributions to chirality mixing operators such as $m_{\rm res}$.

that 3 low-lying modes dominate the s-dependence of this 5d eigenmode.

5. Conclusions

We find that for 3 flavour dynamical DWF simulations, at fixed lattice spacing, the DBW2 gauge action provides only marginal reduction in the residual mass compared with the Iwasaki gauge action. Residual chiral symmetry breaking of $O(10^{-3})$ is achievable with both gauge actions in the region $a^{-1} \geq 1.6$GeV for $L_s \geq 16$. We demonstrate the connection between localised low eigenmodes of the transfer matrix, and a power-law contribution to m_{res}. The presence of low modes creates an indefinite topological index of the chiral Dirac operator, such that both our results for $\rho(0)$ and topological time histories [8] suggest that topology change survives at finer lattice spacings with the Iwasaki action outweighing the gain in residual mass from DBW2.

6. Acknowledgements

We thank Sam Li and Meifeng Lin for help generating the datasets used in this work. We thank Dong Chen, Norman Christ, Saul Cohen, Calin Cristian, Zhihua Dong, Alan Gara, Andrew Jackson, Chulwoo Jung, Changhoan Kim, Ludmila Levkova, Xiaodong Liao, Guofeng Liu, Robert Mawhinney, Shigemi Ohta, Konstantin Petrov and Tilo Wettig for developing with us the QCDOC machine and its software. This development and the resulting computer equipment used in this calculation were funded by the U.S.DOE grant DE-FG02-92ER40699, PPARC JIF grant PPA/J/S/1998/00756 and by RIKEN. This work was supported by PPARC grant PP/G/O/2002/00465 and we thank the University of Edinburgh for providing the facilities essential for the completion of this work.

References

[1] D. B. Kaplan, Phys. Lett. B288, 342 (1992)

[2] M. Golterman, Y. Shamir, Phys.Rev.D68:074501 (2003)
M. Golterman et al, Phys. Rev. D71, 071502 (2005)
M. Golertman et al, Phys. Rev. D72, 034501 (2005)
B. Svetitsky et al, hep-lat/0508015, these proceedings.

[3] P. Hernandez et al, Nucl. Phys. B552, 363 (1999).

[4] S. Aoki, Phys Rev D30, 2653 (1984), S. Aoki, Phys Rev D33, 2399 (1986)
S. Aoki, Phys Rev Lett 57, 3136 (1986)

[5] S. Aoki, Y Taniguchi, Phys Rev D65, 074502 (2002)

[6] CP-PACS, Nucl.Phys.Proc.Suppl. 106, 718 (2002)

[7] Norman Christ, these proceedings.

[8] A. Yamaguchi et al, these proceedings.

[9] K. Hashimoto et al, these proceedings.